PHYSICAL REVIEW B **83**, 020103(R) (2011)

Direct spectroscopic evidence of charge reversal at the $Pb(Zr_{0.2}Ti_{0.8})O_3/La_{0.7}Sr_{0.3}MnO_3$ heterointerface

Chung-Lin Wu,[1,*] Pei-Wei Lee,[1] Yi-Chun Chen,[1] Lo-Yueh Chang,[2] Chia-Hao Chen,[2] Chen-Wei Liang,[3] Pu Yu,[4] Qing He,[4] R. Ramesh,[4] and Ying-Hao Chu[3]

[1]*Department of Physics, National Cheng Kung University, Tainan 70101, Taiwan, Republic of China*

[2]*National Synchrotron Radiation Research Center, Hsinchu 30076, Taiwan, Republic of China*

[3]*Department of Materials Science and Engineering, National Chiao Tung University, Hsinchu 30010, Taiwan, Republic of China*

[4]*Department of Physics, University of California, Berkeley, California 94720, USA*

(Received 25 November 2010; published 21 January 2011)

At the heterointerface of a top ferroelectric $Pb(Zr_{0.2}Ti_{0.8})O_3$ (PZT) ultrathin film and a bottom $La_{0.7}Sr_{0.3}MnO_3$ (LSMO) electrode, we used continuous synchrotron-radiation photoelectron spectroscopy to probe *in situ* and demonstrated that the interfacial charges are reversible and their affected valence-band barrier height becomes modulated upon switching the polarization in the top layer. By monitoring the core-level shifting of the buried LSMO layer under continuous illumination of synchrotron radiation, we directly observed a temporal screening of polarization induced by the photon-generated carriers in the top PZT layer. This dynamic characterization of the core-level shifting of the buried layer demonstrates an effective method to probe the electric conduction and ferroelectric polarization of an ultrathin ferroelectric oxide thin film.

DOI: 10.1103/PhysRevB.83.020103 PACS number(s): 77.55.hj, 77.80.Fm, 79.60.Jv, 73.20.At

Oxide heterojunctions have attracted attention because of their multifunctional properties, which are highly stimulus-sensitive upon coupling with electric, magnetic, or optical fields, and which make them promising candidates for strongly correlated electron devices and highly efficient photovoltaic devices.[1–3] To meet such device applications, understanding and controlling the interfacial phenomena of the oxide heterojunction, at which the interactions of charge, spin, and orbital begin to dominate over the physical properties of the polar oxide interior, has been an area of major progress. To introduce an interfacial charge at the oxide heterojunctions, using a heteroepitaxial technique on oxides, combining various oxides or, especially, alternating the stacking sequence of monolayers to manipulate *polarity discontinuity* at different terminations has produced several prominent examples, including $LaAlO_3/SrTiO_3$,[4–9] $LaTiO_3/SrTiO_3$,[10] $LaVO_3/SrTiO_3$,[11] and ZnO/(Mg,Zn)O[12] heterostructures. These studies demonstrated that a polarity discontinuity would induce interfacial bounded charges and have compensation with mobile charges (electrons or holes) at the heterointerface. However, these interfacial charges determined by termination cannot be further manipulated upon applying external fields. In the ferroelectric oxides, the ferroelectricity provides an additional degree of freedom to manipulate the polarity discontinuity, but knowledge about how the switchable polarization affects the interfacial charges and their corresponding band diagrams of the oxide heterojunctions is lacking. Assisted by the synchrotron-radiation photoelectron spectroscopic (SR-PES) technique, we report here direct evidence of ferroelectric control on interfacial charges (bounded and mobile) and the affected valence-band barrier heights at the oxide heterojunction, which plays an important role in not only the interface physics of oxides but also the design of multifunctional oxide devices.

The photoelectron spectroscopic technique is a powerful tool to obtain direct information about the interfacial electronic structures at a heterojunction with a polarity discontinuity.[7,10,13–16] In particular, using this photon-excited spectroscopic technique to probe an epitaxial heterointerface, the basic issues of the coupling of photon and interfacial charges in the strong correlated oxide heterojunctions might be resolved. We demonstrate here that numerous photon-generated electrons and holes in the top, poorly conductive, ferroelectric oxide layer tend to screen the polarization inside for a long time. Importantly, the polarization screening would diminish the ferroelectric-controlled interfacial mobile charges and eventually vanish under continuous illumination at a ferroelectric heterojunction. This complete polarization screening in an ultrathin ferroelectric film clearly shows an alternative method to separate efficiently the photon-generated electrons and holes, and thereby it displays a distinctive photovoltaic behavior at ferroelectric heterojunctions. The dynamic characterization of polarization screening enables the studies of the electronic transportation and polarization in ferroelectric films that are too thin to be measured with conventional top-electrode methods.

The ferroelectric $Pb(Zr_{0.2}Ti_{0.8})O_3/La_{0.7}Sr_{0.3}MnO_3$ (PZT/LSMO) heterojunction system studied here is particularly suitable for PES measurements, since LSMO is an oxide bottom electrode that not only prevents photoelectron charging but also has good lattice match to diminish the strain and its induced piezoelectric polarization for single-phase PZT growth. We recorded the PES data on a ferroelectric heterojunction sample consisting of a top ultrathin (~4 nm thick, less than the photoelectron escape length of elements in PZT and LSMO) ferroelectric PZT layer and a bottom-electrode LSMO layer (30 nm thick) grown on a $SrTiO_3$ substrate using pulsed laser deposition with the high-pressure reflection high-energy electron diffraction. This ferroelectric heterojunction system has an atomic smooth surface and a downward polarization according to the characterizations of atomic force and piezoresponse force microscopes (AFM/PFM). The PES spectra were recorded using a monochromatic photon source of 380 eV at the scanning photoelectron microscopy (SPEM) end station at the National Synchrotron Radiation Research Center (NSRRC) in Hsinchu, Taiwan, and the accuracy of the energy

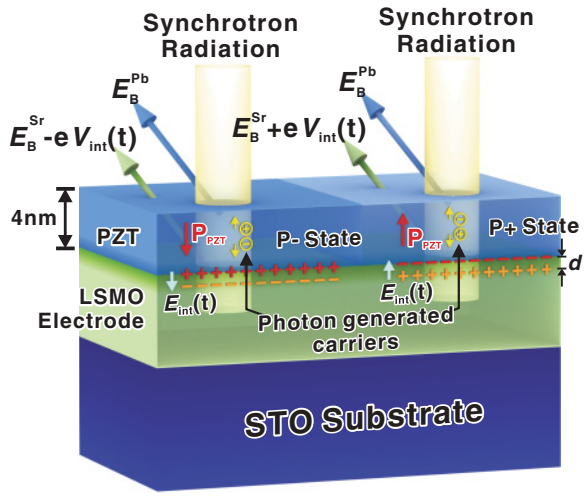

FIG. 1. (Color online) Schematic illustration of our ferroelectric-pattern-assisted SR-PES measurement. The layered structure in the PZT/LSMO heterojunction is shown for the P− and P+ states with the corresponding spontaneous polarization (P_{PZT}) of the top ultrathin PZT film. The sheets of induced bound charges and compensated mobile charges in the LSMO layer, which form the induced E field (E_{int}) across the heterointerface, are shown for both polarization states in this layer structure. The photon-generated electrons and holes would decrease the PZT spontaneous polarization, which is characterized with the Sr core-level binding-energy shift from the buried layer.

position determinations (core-level peaks and valence-band edges) is satisfactory because of the excellent signal-to-noise characteristics in the PES spectra excited by synchrotron radiation.

To investigate the ferroelectric control of interfacial charges, we developed a ferroelectric-pattern-assisted photoelectron-spectroscopy technique, which allows a direct and *in situ* probe of the reversible interfacial electrostatics, as depicted schematically in Fig. 1. In the ferroelectric heterojunction sample with a naturally downward PZT layer, the polarization was reversed by metal probe scanning (probe voltage set to −4 V) to obtain an upward polarization area that is larger than a synchrotron-radiation beam size of about 300 × 400 μm^2. Positive (downward polarization, P− state) and negative (upward polarization, P+ state) bound charge sheets were thus induced at the ferroelectric-electrode heterointerface upon locally switching the polarity discontinuity, leading to an accumulation of mobile electrons and holes in p^+-LSMO (the LSMO epilayer is known to exhibit a high background p-type carrier density). As a result, in distinct ferroelectric patterns with reversed electric configuration, downward and upward interface capacitors were constructed in a separate top sheet of bound charges and a bottom sheet of mobile charges, like the picture shown in a recent x-ray-absorption near-edge spectroscopy (XANES) study.[17] In previous studies, photoelectrons emitted from the buried layer of a heterojunction were particularly sensitive to the discontinuity of an electric field, resulting in an acceleration or deceleration of core-level electrons upon passing through the interface capacitor.[14–17] It should be noted that, under continuous illumination, the internal field of the PZT layer due to bound charges acts as a bias that gradually redistributes the numerous photon-generated carriers (electrons and holes) while the PES spectra are taken, as illustrated in Fig. 1. Therefore, these photon-generated charges would suppress the depolarization field of the PZT and gradually eliminate the polarity discontinuity and induced interface capacitors under continuous light illumination.[18,19] The measured binding energy of the Sr core level from the buried layer thus gradually decreases or increases depending on the downward and upward polarization directions, respectively. This binding energy can be written as $E_B^{Sr}(t) = E_B^{Sr} \pm eV_{int}(t)$, where $eV_{int}(t)$ is the time-dependent potential difference across the interface capacitor, and the concept of that interface capacitor is confirmed by the lack of change in the core-level emission from the top ferroelectric layer.

Figure 2(a) shows the time-dependent Pb 4f and Sr 3d core-level photoelectron spectra in the ferroelectric PZT/LSMO heterojunction sample. These spectra from the buried LSMO layer show that the Sr $3d_{5/2}$ core-level energy shift increases and decreases exponentially with the duration of SR illumination [Fig. 2(b)], which is associated with an exponential decrease of induced interface capacitors accompanied by

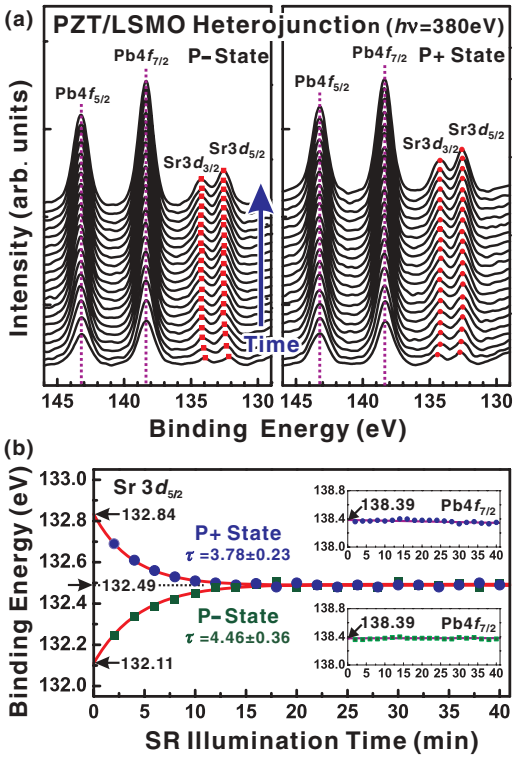

FIG. 2. (Color online) (a) Time-dependent photoelectron spectra of P− and P+ states in a PZT/LSMO heterojunction sample obtained at an incoming photon energy of 380 eV within 90 min. In the detected photoelectron energy range, the peak position of the Sr 3d core level is relative to that of the Pb 4f core level as a function of Sr illumination time and of the P− and P+ states. (b) The evolution of the Sr 3d binding-energy positions was reversed for the P− and P+ states and fitted to the function $\Delta E e^{-t/\tau}$, in which ΔE is a fitting constant and τ is a time constant. The positions of Pb 4f binding energy (shown in the inset) are nearly constant with SR illumination time.

the polarization screening with photon-generated carriers. It should be noted that the Sr core-level shifting behavior in upwardly and downwardly oriented interface capacitors is nearly symmetric at the same saturated position of 132.49 eV, representing a complete screening of both polarizations in the PZT layer upon a sufficient number of carriers. This suggests that a single-phase ultrathin PZT film has the capability to separate effectively photon-generated electrons and holes to display a conventional photovoltaic effect. As expected, there is no detectable change in Pb 4*f* core levels from the top PZT layer for both P− and P+ states (Pb 4 $f_{7/2}$ at around 138.39 eV), as shown in the inset of Fig. 2(b).

The dynamic characterization of interface capacitors associated with Sr core-level shifting is coupled via the mobility of photon-generated carriers, from which the electric conductivity of mobile carriers in PZT is calculated. According to electrodynamics, the dynamic behavior is modeled as a charged dielectric capacitor with charge leakage. The potential drop in terms of $eV_{\text{int}}(t)$ is expected to display an exponentially temporal decay according to the relationship of $\Delta E e^{-\mathbf{t}/\tau}$, in which ΔE is a fitting parameter and $\tau$is the relaxation time constant. Thus, the Sr $3d_{5/2}$ core-level shifting can be simulated by the formula $E_B^{\text{Sr}}(t) = E_B^{\text{Sr}} + \Delta E e^{t/\tau}$. For two polarization directions, that is, two interface capacitor orientations, the time constants derived from curve fitting were 4.46 ± 0.36 min (P− state) and 3.78 ± 0.23 min (P+ state). From the leaking capacitor model, the time constant can be simulated from the relative permittivity and conductivity using $\tau = \varepsilon/\sigma$; the relative permittivity ε of the epitaxial PZT film is about 300. Thus, the conductivities of photon-generated carriers σ in the ultrathin PZT film are $(9.99 \pm 0.81) \times 10^{-14}$ S/cm (σ_{P-} for the P− state) and $(11.75 \pm 0.72) \times 10^{-14}$ S/cm (σ_{P+} for the $P+$ state) at room temperature, which are similar to the results of thermal-activated and extrinsic- and/or intrinsic-doping charge transportation.[20–22] In addition, the conductivity increases slightly after polarization flipping ($\sigma_{P+} > \sigma_{P-}$), in agreement with the results of generating oxygen vacancies.[23,24]

In addition, the maximum potential drop of the interface capacitor was obtained at ΔE values of -0.38 ± 0.02 eV (P− state) and 0.35 ± 0.01 eV (P+ state). From the geometry of the interface capacitor, the spontaneous polarization is described with a relation $P_{\text{PZT}} = \varepsilon_{\text{LSMO}} \Delta V/d$, in which $\varepsilon_{\text{LSMO}}$ is the permittivity of epitaxial LSMO, ΔV is the potential drop of the interface capacitor (from the fitting parameter $\Delta E/e$, i.e., 0.38 V for the P− state and 0.35 V for the P+ state), and d denotes the length of electron accumulation and depletion on the LSMO side (shown in Fig. 1) and is theoretically obtained in LSMO to be about 0.3 nm.[25,26] Thus, the spontaneous polarizations of PZT are 33.63 μC/cm^2 (P− state) and 30.10 μC/cm^2 (P+ state), which are close to the result of spontaneous polarization on the value of about 30 μC/cm^2 in the 4-nm film of PZT [27]. The determinations of conductivity and polarization in an ultrathin PZT film associated with its induced interface capacitor are addressed here without the use of surface electric contacts.

To obtain the valence-band barrier height of the PZT/LSMO heterojunction, the PES spectra of PZT and LSMO epilayers (both with thicknesses of about 50 nm, as shown in Fig. 3) are required to reveal the respective core-level (CL) energies relative to their valence-band maxima (E_{VBM}). The relationship between the valence-band barrier height ΔE_v (absolute value) and the measured PES results is[15]

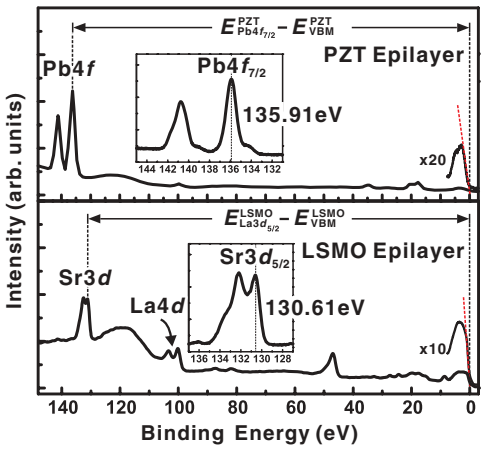

FIG. 3. (Color online) Photoelectron spectra of PZT and LSMO bulk epilayers for measurements of valence-band barrier height of the PZT/LSMO heterojunction. The energy differences between the represented core levels (Sr $3d_{5/2}$ for LSMO and Pb 4 $f_{7/2}$ for PZT) and the valence-band maxima (shifted to zero) were derived from these spectra.

$$\Delta E_v = \left(E^{\text{LSMO}}_{\text{VBM}} - E^{\text{LSMO}}_{\text{Sr}\,3d_{5/2}}\right)_{\text{LSMO}} - \left(E^{\text{PZT}}_{\text{VBM}} - E^{\text{PZT}}_{\text{Pb}\,4f_{7/2}}\right)_{\text{PZT}} + (\Delta E_{\text{CL}})_{\text{PZT/LSMO}}, \quad (1)$$

where $(\Delta E_{\text{CL}})_{\text{PZT/LSMO}}$ is the energy separation between Pb 4 $f_{7/2}$ and Sr $3d_{5/2}$, determined in Fig. 2. The resulting values

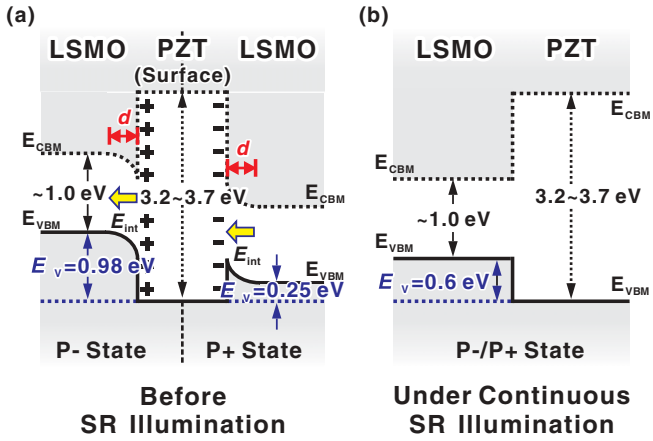

FIG. 4. (Color online) Schematic band diagrams of a PZT/LSMO ferroelectric heterojunction derived from *in situ* SR-PES measurements (a) before and (b) after Sr illumination. The electric field (E_{int}) inside the interface capacitor produces a potential drop in the region of thickness d. Downward and upward interface band-bending structures correspond to different induced charges (P− and P+ states) before SR illumination. Under continuous SR illumination, a flat-band structure is obtained with complete screening of polarization in the PZT layer of the P− and P+ states.

for the two epilayer samples are $E^{\mathrm{PZT}}_{\mathrm{VBM}} - E^{\mathrm{PZT}}_{\mathrm{Pb}\,4f_{7/2}} = 135.91 \pm 0.02$ eV and $E^{\mathrm{LSMO}}_{\mathrm{VBM}} - E^{\mathrm{LSMO}}_{\mathrm{Sr}\,3d_{5/2}} = 130.61 \pm 0.03$ eV. Using Eq. (1) and assuming band-gap energies for PZT of 3.2–3.7 eV and for LSMO of about 1 eV,[28,29] the band diagrams of the ferroelectric PZT/LSMO heterojunction, which depends on the polarization state and SR illumination time, are illustrated in Fig. 4 as a type-I band alignment. The electric field (E_{int}) within the interface capacitor produces a potential drop inside the capacitor region of thickness d, and shifts the relative positions of the valence and conduction bands of LSMO outside the capacitor. The band diagram thus reveals that the P− state of the PZT/LSMO heterojunction has a larger barrier height value of 0.98 eV [$(\Delta E_{\mathrm{CL}})_{\mathrm{PZT/LSMO}} = 6.28$ eV], which implies a downward band-bending structure for electron accumulation at the heterointerface. In contrast, the P+ state has a smaller barrier height value of 0.25 eV [$(\Delta E_{\mathrm{CL}})_{\mathrm{PZT/LSMO}} = 5.55$ eV], which implies an upward band-bending structure for hole accumulation (i.e., electron depletion) at the heterointerface. These results show that the valence-band barrier height of the PZT/LSMO heterojunction can be modulated with more than 0.7 eV as a result of the polarization reversal in the top PZT layer. Furthermore, under complete polarization screening in PZT with long-time SR illumination, both P+ and P− heterointerfaces are charge-equivalent and have the same barrier height value of 0.6 eV [$(\Delta E_{\mathrm{CL}})_{\mathrm{PZT/LSMO}} = 5.90$ eV] with the flat-band diagram having no E_{int} influences, as shown in Fig. 4(b).

In summary, a ferroelectric-pattern-assisted PES study was conducted on a PZT/LSMO heterojunction to investigate the reversible interfacial charges. Mobile electrons and holes and their corresponding band bending clearly occur in the electrode LSMO layer with respect to the polarization direction of the top ferroelectric PZT layer. Using time-dependent PES measurements, we observed that interfacial electrons and holes exponentially decaying to zero were responsible for the complete polarization screening by photon-generated charges in the top PZT layer. This dynamic investigation of polarization screening can also be used to measure the electric and ferroelectric properties of top ultrathin ferroelectric layers without the surface electrode's help.

This work was supported by the National Science Council in Taiwan.

*Electronic address: clwuphys@mail.ncku.edu.tw

[1] H. Takagi and H. Y. Hwang, Science **327**, 1601 (2010).
[2] S. Y. Yang *et al.*, Nat. Nanotechnol. **5**, 143 (2010).
[3] M. Qin, K. Yao, and Y. C. Liang, Appl. Phys. Lett. **95**, 022912 (2009).
[4] A. Ohtomo and H. Y. Hwang, Nature (London) **427**, 423 (2004).
[5] W. Siemons, G. Koster, H. Yamamoto, W. A. Harrison, G. Lucovsky, T. H. Geballe, D. H. A. Blank, and M. R. Beasley, Phys. Rev. Lett. **98**, 196802 (2007).
[6] K. Yoshimatsu, R. Yasuhara, H. Kumigashira, and M. Oshima, Phys. Rev. Lett. **101**, 026802 (2008).
[7] O. Copie *et al.*, Phys. Rev. Lett. **102**, 216804 (2009).
[8] T. Fix, F. Schoofs, J. L. Driscoll-MacManus, and M. G. Blamire, Phys. Rev. Lett. **103**, 166802 (2009).
[9] M. Sing *et al.*, Phys. Rev. Lett. **102**, 176805 (2009).
[10] A. Ohtomo *et al.*, Nature (London) **419**, 378 (2002).
[11] Y. Hotta, T. Susaki, and H. Y. Hwang, Phys. Rev. Lett. **99**, 236805 (2007).
[12] A. Tsukazaki A. Ohtomo, T. Kita, Y. Ohno, H. Ohno, and M. Kawasaki, Science **315**, 1388 (2007).
[13] R. W. Grant, J. R. Waldrop, and E. A. Kraut, Phys. Rev. Lett. **40**, 656 (1978).
[14] G. Biasiol, L. Sorba, G. Bratina, R. Nicolini, A. Franciosi, M. Peressi, S. Baroni, R. Resta, and A. Baldereschi, Phys. Rev. Lett. **69**, 1283 (1992).
[15] C.-L. Wu , H.-M. Lee, C.-T. Kuo, S. Gwo, and C.-H. Hsu, Appl. Phys. Lett. **91**, 042112 (2007).
[16] M. Takizawa *et al.*, Phys. Rev. Lett. **102**, 236401 (2009).
[17] C. A. F. Vaz, J. Hoffman, Y. Segal, J. W. Reiner, R. D. Grober, Z. Zhang, C. H. Ahn, and F. J. Walker, Phys. Rev. Lett. **104**, 127202 (2010).
[18] H. N. Al-shareef, D. Dimos, W. L. Warren, and B. A. Tuttle, Int. Ferroelectr. **15**, 53 (1997).
[19] M. Grossmann *et al.*, J. Appl. Phys. **92**, 2680 (2002).
[20] J. Lappalainen and V. Lantto, Phys. Scr. T **79**, 220 (1999).
[21] B. A. Boukamp, M. T. N. Pham, D. H. A. Blank, and H. J. M. Bouwmeester, Solid State Ion. **170**, 239 (2004).
[22] J. G. Burt and R. A. Krakowski, J. Am. Ceram. Soc. **54**, 415 (1971).
[23] R. Ramesh, *Thin Film Ferroelectric Materials and Devices* (Kluwer Academic, Boston, 1997), p. 203.
[24] S.-H. Kim, Y.-S. Choi, C.-E. Kim, and D.-Y. Yang, Thin Solid Films **325**, 72 (1998).
[25] X. Hong, A. Posadas, and C. H. Ahn, Appl. Phys. Lett. **86**, 142501 (2005).
[26] Y. Hikita, M. Nishikawa, T. Yajima, and H. Y. Hwang, Phys. Rev. B **79**, 073101 (2009).
[27] C.-L. Jia *et al.*, Nat. Mater. **6**, 64 (2007).
[28] I. Boerasu *et al.*, J. Appl. Phys. **93**, 4776 (2003).
[29] K. Zhao *et al.*, Appl. Phys. Lett. **88**, 141914 (2006).